Mar 7th, 8:00 AM

Optical Subcarrier Communications

J. H. Ward
ITT Federal Laboratories

M. L. Shechet
ITT Federal Laboratories

J. H. Ward III
M. L. Shechet

ITT Federal Laboratories, San Fernando, California

Summary

This paper discusses the use of rf subcarriers placed on optical beams for communication purposes. Through the use of advanced optical beam processing and post detection electronic processing, the advantages of optical frequency techniques can be combined with the mature background of the rf technology. These techniques are expected to find applications for long range wideband communication, spacecraft tracking and rendezvous, and altimetry, as well as for aircraft and spacecraft landing aids.

Introduction

There is currently considerable enthusiasm over the application of the laser in optical radar and communication systems. Undoubtedly, optical frequencies will have increasingly greater importance in communications as more powerful and coherent sources become available. The basic advantage of optical frequency communications over microwaves is the combination of narrow beamwidths with potentially large information bandwidth. Both of these properties are due to the high frequencies associated with optical radiation. It is significant that these advantages should also lead to the primary disadvantages. In particular, narrow beamwidth means that the target must be located and tracked with extraordinarily high accuracy. A further hindrance to communications at optical frequencies is the atmospheric effect on the light beam. This limitation is particularly severe on systems which require the preservation of the spatial coherence of the beam for certain information processing functions.

One of the simplest ways to exploit the large information bandwidth of an optical carrier is to place rf subcarriers on the optical beam which can, in turn, be modulated.

The subcarrier approach to optical communications permits the use of a variety of established data processing techniques and may assume many levels of sophistication, depending upon the particular mission to be performed. With appropriate post detection electronic processing, the following missions may be accomplished:

- o Distance and velocity measurement,
- o Angle measurement and tracking,
- o Phase-locked receiver tracking,
- o Multichannel telemetry,
- o Television.

The use of optical beams in these missions requires a careful consideration of the optical-electronic interface. In particular, the modulation of the beam and its effect on photodetection devices must be examined.

First, it is necessary to consider the optical beam as a carrier. Although the laser oscillator may be considered quite coherent optically, it is not coherent in the absolute sense and, indeed, has a spectral width of several kilocycles under ordinary conditions. It is evident that an optical beam must be treated as a noisy carrier for communication purposes. In addition, further analysis must be given to generation of shot noise by a photodetector excited by a modulated laser beam.

This laboratory investigated the effects of a noisy carrier on conventional techniques of synchronous detection by phase-locking to a microwave subcarrier placed on an optical beam having a spectral width of approximately 10^6 gigacycles.[1] The outcome of this investigation demonstrated that the self-noise associated with a wideband optical carrier does not require drastic modification of conventional synchronous detection techniques. This suggests the possibility of synchronous detection of rf subcarriers on noisy optical beams, thereby gaining most of the advantages afforded by synchronous detection.

In the presentation which follows, the modulation process and the derivation of a generalized signal-to-noise ratio equation are discussed. In addition, three subcarrier systems developed at our laboratory are described. These are range and angle tracking systems and a prototype optical receiver.

Modulation

A necessary task in synthesizing an optical communication system is the placing of the information on the light beam. The current need for wideband communications has resulted in a critical requirement for microwave light modulators to fully exploit the bandwidth potential of lasers. Although there are numerous methods of modulating light beams at low frequencies, few are practical at radio frequencies. The most generally useful of the optical modulator techniques employ the linear electro-optic effect in certain crystals. The electro-optic effect refers to the alteration of refractive properties of an optical medium by the application of an electric field. As a result of this effect, an electrically variable phase retardation may be produced in a light beam upon its transit through the electro-optic medium. All electro-optic modulators using transparent media are basically phase modulators in that the modulating fields act directly to change the optical phase velocity of the medium.

Electro-optic materials fall into two classes. The first comprises materials which exhibit a linear electro-optic effect, and the second includes materials which possess a quadratic electro-optic effect. The specific materials considered in the first class are either crystals of cubic symmetry, such as cuprous chloride and zinc sulfide, or crystals of the tetragonal scalenohedral symmetry, such as potassium dihydrogen phosphate (KDP) and its isomorphs. Considerable progress is being made in the development of new materials. However, it is difficult to obtain sufficiently strain-free optical quality samples. This discussion is concerned with the application of the tetragonal materials and, specifically, with KDP because of the availability of large, high quality samples.

The scope of this paper does not permit a detailed treatment of the electro-optic effect. However, a brief qualitative explanation is in order so that the basic design considerations may be appreciated. Those who are

interested in a more detailed discussion are referred to a previous paper by the author,[2] or to the original work of Billings.[3]

In the absence of an electric field, a crystal of the tetragonal class, such as KDP, is uniaxial. When an electric field is applied, the crystal becomes biaxial, having induced axes which are not generally coincident with the normal crystallographic axes. The results of an electric field applied along the optical axis (the z axis) are of special interest. In this case, the z and z' axes are coincident, and the induced x' and y' axes are rotated 45° from the x and y crystallographic axes. The magnitude of the axes rotation angle is independent of the magnitude of the applied field for this case. Figure 1 shows a prism of KDP having faces respectively perpendicular to the induced x', y', z' axes. It can be shown that the refractive indices for polarization vectors along the induced axes are given by equations (1), (2), and (3)

$$n_{x'} = n_o + \frac{1}{2} n_o^3 r_{63} E_z(t) \qquad (1)$$

$$n_{y'} = n_o - \frac{1}{2} n_o^3 r_{63} E_z(t) \qquad (2)$$

$$n_{z'} = n_e \qquad (3)$$

where n_o and n_e denote the ordinary and extraordinary index of refraction, r_{63} is the electro-optic coefficient having dimensions of centimeters per volt, and $E_z(t)$ is the value of the electric field applied in the z direction. It is obvious that the induced birefringence is greatest for light propagating in the z direction parallel to the electric field, and that natural birefringence does not occur for this case. The phase difference in radians for the two normal polarization directions is given by

$$\Delta\varphi = \frac{2\pi\, n_o^3\, r_{63}\, d\, E_z(t)}{\lambda}, \qquad (4)$$

where d is the thickness of the crystal in the direction of propagation, and λ is the wavelength of the light.

Equation (4) can be written in terms of the applied voltage, V, as

$$\Delta\varphi = \frac{2\pi\, n_o^3\, r_{63}\, V(t)}{\lambda}. \qquad (5)$$

The phase difference is, therefore, directly proportional to the potential difference and is independent of the crystal thickness for the longitudinal field case. The form of the modulation depends upon the input beam polarization state. If the input beam is circularly polarized or linearly polarized having an orientation at 45° to the x' and y' axes, the output beam will be elliptically polarized in general, because of the relative retardation produced between the two normal components of polarization. The ellipticity of the output beam polarization is dependent upon the applied electric field. This polarization modulation can be converted to an intensity modulation by passing the output through a properly oriented polarizer.

If light is propagated normal to the electric field in the y' direction, as illustrated in Figure 2, the relative retardation for polarization components in the z' and x' directions is given by

$$\Delta\varphi = \frac{2\pi(n_o - n_e)}{\lambda} + \frac{\pi\, n_o^3\, r_{63}\, S\, V_z(t)}{\lambda\, d} \qquad (6)$$

where S is the length of the crystal in the propagation direction, and d is the thickness of the crystal in the direction of the applied field. In the transverse field case, the retardation is directly proportional to the path length in the crystal and to the magnitude of the applied voltage. The first term in the transverse field equation represents the natural birefringence and the second term indicates the field dependent retardation. Because of the natural birefringence associated with this direction of propagation, it is necessary to use monochromatic light of low divergence. One of the more serious problems is associated with the field independent term, since it is very sensitive to environmental changes. It is possible to construct a modulator which is thermally compensated by using two matched crystals of the proper orientation, as suggested by Peters.[4]

By confining the polarization vector of the input beam to the x' direction for light propagating in the y' direction, it is possible to accomplish a pure phase modulation of the light beam. This form of modulation is least susceptible to random strains in the crystal structures. It has been determined experimentally, however, that the maximum power which can be dissipated in the crystal is approximately 1 watt, because of thermally induced strains.

Figure 3 shows an experimental model of a modulator of the transverse field type constructed at this laboratory. The modulator is of the partially dielectric loaded coaxial type with input and output connectors for matched operation. The coaxial package illustrated in Figure 4 is designed to match the modulating field phase velocity with the optical group velocity in the electro-optic crystal. Figure 5 shows the performance of a modulator having a crystal length of 6 cm, matched to a current driver through a simple parallel tuned circuit resonating at 100 mc. The variation of modulation depth with frequency is shown for two matching circuits dissipating 5 watts and having different Q's.

Truly efficient broadband performance can be achieved by a continuous interaction in a structure where both the modulating and optical signals can propagate as TEM waves having equal phase velocities. Such conditions permit the use of long crystals with a concomitant increase in modulation efficiency. Modulators of this type have been constructed which are capable of efficient modulation over gigacycle bandwidths. Such bandwidths can best be utilized, under the present state-of-the-art limitations in electronic systems, through optical subcarrier multiplexing.

Signal-to-Noise Power Ratio

The performance of an optical communication system is usually determined through a consideration of the signal-to-noise power ratio at the output of a photodetector. Expressions for the signal-to-noise power ratio up to this time have been based on very simple and restrictive models for the input optical beam. Such signal-to-noise expressions may be inadequate for handling the laser beam or, more specifically, the modulated laser beam. A completely general expression for the power density spectrum at the photodetector output has been

developed[5] at this laboratory which predicts system performance for any input optical beam characteristics.

The approach leading to the development of the signal-to-noise power ratio expression was to compute the power density spectrum at the output of a photodetector in a completely general fashion. Figure 6 illustrates the various components and mechanisms considered in the derivation. Thermal noise, which appears as an additive term, is not considered in the derivation. This omission does not seriously affect the generality of the power density expression. No restrictions are imposed on the nature of the light source; that is, it may have any beam statistics. The forms of modulation are equally nonrestrictive and may be of the amplitude or angle type, providing the proper demodulation scheme is used. External Gaussian noise inputs shaped by the optical prefilter are considered. The optical prefilter may be a simple narrowband filter or some more complex arrangement, such as an interferometric comb filter, described in a later section. The photodetector is considered a square law device followed by a Poisson mechanism with filtering. The latter filter represents the spectral response of the photodetector or the post detection electronics. In addition to the effects of optical inputs, the shot noise associated with the dc potential or dark current is considered.

The development of this expression utilizes the basic assumption of Poisson statistics for photoemission and considers the noise generation as a result of driving one probabilistic process, which is the shot effect, with another probabilistic process, which is the input optical beam. The power density spectrum of the output of the detector has contributions which may be classified as signal cross signal, noise cross noise, signal cross noise, and shot noise.

The scope of this paper does not permit a detailed derivation of the general output power density spectrum. However, the amplitude modulated case is presented as a specific and useful example. Assuming a signal bandwidth such that spectral shaping by the photodetector response can be neglected, the signal and noise terms can be collected and written in the form of equation (7).

$$\text{Signal-to-noise power ratio} = \frac{\left(\frac{\eta}{\Delta E}\right)^2 (P_S)^2 \left(\frac{k}{1+\frac{k^2}{2}}\right)^2}{\Delta f\left\{\left(\frac{\eta}{\Delta E}\right)^2 (2\pi)\left(\frac{1}{\Delta\nu}\right)\left[P_N{}^2 + \frac{1}{2} P_S P_N\left(\frac{k^2}{1+\frac{k^2}{2}}\right)\right] + \left(\frac{\eta}{\Delta E}\right)\left[P_S + P_N\right] + N_O\right\}} \qquad (7)$$

where
- η = photodetector quantum efficiency
- ΔE = energy per photon in optical bandpass
- k = amplitude modulation index
- $\Delta\nu$ = optical prefilter bandwidth in cps
- Δf = electronic post detection bandwidth
- P_S = total power in signal beam on detector
- P_N = total power in background on detector
- N_O = dark current parameter or average number of photoelectrons per unit time emitted from photocathode.

The noise portion of the equation consists of three distinct terms. The first is the higher order correlation term which arises from the quadratic detection process and consists of a noise-cross-noise term and a noise-cross-signal term. The second and third terms are shot noise due to the total power in the optical beams and the dc potential or dark current respectively. It is significant to note that the higher order correlation terms, which in the past have been neglected in predicting optical system performance, become significant under conditions of narrow optical prefilter bandwidth and in the presence of high optical power levels, such as might be experienced in optical heterodyning. As an example, a prefilter bandwidth of 1 Angstrom, which is not uncommon in the present state-of-the-art, produces a quadratic noise equivalent in magnitude to the shot noise for a power level of 10^{-7} watt on the photodetector. Although this power level is not generally encountered in practice, the quadratic noise term becomes more significant with narrower optical prefilters. The future use of optical prefilters of less than 1 Angstrom bandwidth are feasible through the application of electro-optical networks.

Prototype Optical Subcarrier Systems

Three systems are now presented which incorporate the techniques discussed above. These are a ranging system, a space rendezvous system, and a multiplex optical receiver.

EODARS

A natural adjunct to the development of optical subcarrier methods is the combination of narrow optical beams and precision phase measurement techniques. These two complimentary techniques have been combined in a concept of EODARS—an acronym for Electro-Optical Direction and Ranging Systems. The breadboard configuration for the ranging section of the EODARS is shown in Figure 7. This system is illustrated by the simplified block diagram in Figure 8. Distance measurement is accomplished through a comparison of the phase of a transmitted rf subcarrier placed on the optical beam with that same signal returned from a target. The advantage of using cw subcarrier techniques over pulse operation for ranging is that range measurements can be made to zero distance. Accurate short range measurements are necessary for such missions as space rendezvous and docking and low level altimetry.

The prototype EODARS is a single channel system with an unambiguous range of approximately 100 feet. A system is under development which is capable of ambiguity resolution over greater distances through the use of multiple channels. The prototype system utilizes digital phase comparison techniques to achieve relative phase angle measurements to an accuracy of 1/4000, under conditions of good signal-to-noise ratio. An absolute accuracy of 0.1 inch has been demonstrated in the single channel breadboard system over the full range down to zero.

The transmitter portion of the systems consists of a gallium arsenide injection source, directly modulated at 5 megacycles, and refractive beam forming optics which direct the beam onto the target whose range is to be determined. A portion of the light reflected by the target is collected by the receiving lens and is directed by a beamsplitter onto a photomultiplier detector after passing through an optical prefilter and a background limiting field stop. The transmitting and receiving optical systems are made coaxial for use with both diffuse and cooperative targets.

The reference oscillator produces the basic modulation tone of 5 megacycles and establishes the zero phase reference. The amplified 5 megacycle signal directly modulates the optical source. The modulated light traverses the distance between the optical transmitter and the target, and returns to the optical receiver,

producing a second 5 megacycle signal with a phase shift which is proportional to the total distance traveled. The purpose of the data mixer is to translate this phase shift of the 5 megacycle signal to a lower frequency, nominally 1.22 kc, to facilitate phase measurement. The second input to the data mixer is a 5 megacycle signal offset phase coherently by 1.22 kc. This signal is generated in the offset reference generator which is a phase locked loop utilizing two inputs. One of the inputs is the 5 megacycle reference, and the other is a phase coherent 1.22 kc signal. The phase shift between these inputs represents the distance traveled by the light beam which is twice the distance between the target and the receiver. The system readout is a simple counter which is started by the leading edge of the reference signal and stopped by the leading edge of the data signal. The phase angle readout is calibrated to give a direct measure of the distance between a reference on the transceiver and the target. The accuracy of the readout is related to the signal-to-noise ratio according to equation (8)

$$\sigma = \frac{1}{\pi^2}\sqrt{\frac{1}{2(S/N)}} \text{ parts per cycle .} \qquad (8)$$

Figure 9 shows this relationship for a one σ accuracy in parts per cycle for a single channel system. The experimental performance of the breadboard system was 12 db below that initially predicted by the previously described S/N equation. The discrepancy was found to be caused by a lower optical power output from the source than that suggested by the manufacturer. Measurements indicate that the rise times quoted for pulsed operation by diode manufacturers are associated with higher current densities than can be realized in continuous operation and, consequently, do not permit the expected higher frequency operation. The diode output seems to follow a 6 db per octave fall-off above 1 megacycle. Making the proper correction for optical efficiency at the source, the analytical and experimental performance are in good agreement, as shown in Figure 10.

In static measurements, the range accuracy can be improved by performing a time integration or an averaging over many cycles of data. By using multiple channels and higher subcarrier frequencies, measurements in range to one part in several million are feasible. These same optical subcarrier digital processing techniques can be used with more powerful laser sources and more sophisticated electro-optical "front ends" to achieve high accuracy measurements over great distances.

Optical Rendezvous

Some of these optical subcarrier data processing techniques have been employed in the prototype Optical Rendezvous Guidance System shown in Figure 11. This system was developed under the direction of the NASA/Marshall Space Flight Center. Figure 12 gives the system performance specifications.

Figure 13 is a block diagram of a prototype optical guidance system, including assemblies for both the target vehicle and for the chaser vehicle. The system operates in both an acquisition and tracking mode.

A wide angle telescope and sensor on the chaser vehicle detects the relatively wide beam acquisition light source on the target vehicle. The sensor is an ITTFL multiplier phototube, which is capable of electronically scanning an acquisition field of view.

When the beacon comes into the chaser's acquisition field, this system locates the target beacon by means of a raster scan, and acquisition occurs. The sensor automatically switches to the tracking mode and generates angular information to cause the chaser vehicle to align itself with the beacon located on the target vehicle. The long range laser light source of the chaser vehicle illuminates the target vehicle. This allows the tracking system on the target vehicle to acquire the chaser vehicle light source. The target vehicle then aligns itself with the chaser vehicle. In the aligned position, the chaser vehicle tracking system operates with a passive reflector on the target vehicle.

The receiving optics on the chaser vehicle consist of a wide angle system for acquisition and a narrow angle, long focal length system for accurate tracking. The two are coaxial and use the same tracking error sensor to generate the tracking signals.

The long range system is designed for operation to 120 Km and uses a gallium arsenide laser transmitter, operated in a pulsed mode. Range is determined by measuring the time for a light pulse to travel from the source to the reflector and return. For short ranges, the cw subcarrier approach is utilized to obtain accurate measurements of range and range rate. This mode begins at 3 km and continues until docking is completed. The range measurements are made by phase comparison between the modulation of the transmitted signal and the modulation received from the retroreflector. The accuracy of this measurement is approximately 10 centimeters.

Homodyne Receiver

A more sophisticated approach to optical subcarrier processing is embodied in the optical homodyne system. This system is capable of accomplishing various missions, including voice and TV multiplexing and telemetry, electronic phase-locking, and electronic phase comparison through the use of optical frequency mixing and advanced electronic processing techniques.

The optical section of the receiver is a type of time delayed autocorrelator which is a familiar technique used at radio frequencies for demodulation of phase modulated signals. The optical autocorrelator is shown schematically in Figure 14 in which an entering optical beam, denoted by $X(t)$ is split into two beams. The amplitudes of the optical beam which impinge on the side channel photodetectors are denoted by $x(t)$ and $x(t + \tau)$ for the nondelayed and delayed beams, respectively. A portion of the two side channel beams are combined, giving rise to an input of $x(t) + x(t + \tau)$ to the central photodetector. Photodetection produces an output proportional to the intensities of the input beams yielding an $x(t)^2$ and an $x(t + \tau)^2$ output in the respective side channels and an $x(t)^2 + 2x(t)x(t + \tau) + x(t+\tau)^2$ output in the central channel. The signals from the photodetectors in the side channels are subtracted from the output of the central channel photodetector to remove unwanted correlated contributions in the central channel, leaving only the autocorrelation term. It should be pointed out that the side channel contributions are significant only when the so-called rf or quadratic noise predominates. As mentioned earlier, this might be the case under conditions of high total optical power and/or very narrow optical bandwidths. This arrangement of a split beam interferometer with three photodetectors and addition-subtraction circuits is an electro-optical autocorrelator.

It is possible to "mix in" a locally generated subcarrier with the incoming optical beam by the addition of an electro-optical modulator in one arm of the interferometer, as illustrated in Figure 15. The addition of the local modulator may be considered qualitatively as producing a shift in the central channel interference pattern which is proportional to the phase shift induced in the local modulator by an electric field. This fringe intensity variation is superimposed on the original incoming beam, and is mixed with the incoming beam in

the square law photodetection process. By placing the local electro-optical modulator in one arm of the interferometric arrangement, a phase-to-amplitude conversion for this related modulation is not required. The interferometric time delay may, therefore, be set so as to optimize the phase-to-amplitude conversion of the modulation placed on the beam at the transmitter. In practice, the optical path length difference of the interferometric arrangement should be of the order of one-half wavelength corresponding to the transmitter subcarrier frequency.

It can be shown that the frequency translated output signal is proportional to the Bessel function product shown in equation (9)

$$J_1(k_r)^2 \, J_1\left(2k_t \sin \frac{\nu\tau}{2}\right)^2 , \qquad (9)$$

where k_r = the modulation index of the local receiver modulator

k_t = the modulation index of the transmitter modulator

ν = the transmitted subcarrier frequency

τ = the interferometric time delay.

This function is optimized for a phase modulation index corresponding to the first Bessel zone maximum of approximately 1.8 radian.

Figure 16 shows the breadboard electro-optical "front end" with local modulator, as described above. This unit is an optical frequency mixer-demodulator for phase modulated light. A breadboard system of this type has been demonstrated in the laboratory by phase-locking to the optical subcarrier difference frequency appearing at the output of the central channel photodetector. In this experiment, a 105 megacycle subcarrier placed on the transmitter beam was mixed in the receiver with a 30 megacycle optical subcarrier introduced by the receiver local modulator. The expected mixing components were observed at the central channel output, and the 135 megacycle sum component was phase-locked by means of the ITTFL 4004 phase-locked tracking receiver.

A video communication experiment is illustrated in Figure 17. In this experiment a gas laser beam is phase modulated with a 105 megacycle subcarrier containing video information. A portion of the modulated transmitter beam is collected by the receiving optics and enters the "front end" interferometer. The local electro-optical phase modulator superimposes a spectrally pure 30 megacycle subcarrier which mixes with the incoming 105 megacycle subcarrier containing the video information. The 135 megacycle sum component at the central channel is inserted into the ITTFL Model 4004 phase-locked tracking receiver which phase-locks to the subcarrier tone and translates the video to a 45 megacycle IF for processing and display in a conventional TV monitor.

Preparations are in progress for field testing of the optical communication link over a three mile distance between the laboratory and a nearby mountain range.

Figure 18 shows the electro-optical transmitter consisting of a HeNe laser source, transverse field phase modulator, and beam forming telescope. A bore-sighted spotting scope is included to facilitate pointing. The "front end" section of the optical receiver is shown mounted on a 24 inch diameter collecting aperture in Figure 19.

Conclusion

The preceding material has presented some of the basic techniques for optical subcarrier communications, as well as a discussion of three systems utilizing these techniques. The main thought that we would like to leave with you is that the use of subcarriers on an optical beam provides a great measure of versatility. It has advantages for a number of space-oriented missions, including long range, wideband communication, spacecraft tracking and rendezvous, and spacecraft altimetry and landing aids. It also allows the use today of well-developed rf techniques combined with the advantages of the newer electro-optical technologies.

References

1. J. H. Ward, et al., "Synchronous Detection of Microwave-Modulated Incoherent Optical Carriers," Proc. IEEE (correspondence), 52, p. 854, July 1964.
2. J. H. Ward, "The Transverse Field Electro-Optical Modulator," ITTFL Technical Memorandum 65-103.
3. B. H. Billings, "The Electro-Optic Effect in Uniaxial Crystals of the Type X H_2PO_4," Journal of the Optical Society of America 39, p. 797, October 1949.
4. C. J. Peters, "Gigacycle-Bandwidth Coherent-Light Traveling-Wave Amplitude Modulator," Proc. IEEE 53, p. 455, May 1965.
5. W. F. Davison, "Shot Noise in Optical-to-Electric Converters," ITTFL Technical Memorandum 63-239.

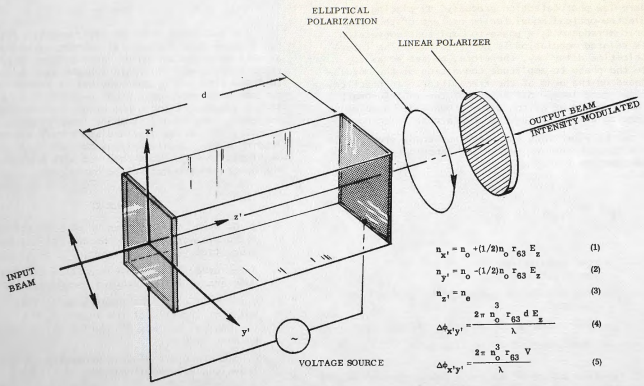

Figure 1 Longitudinal Field Electro-Optical Modulator

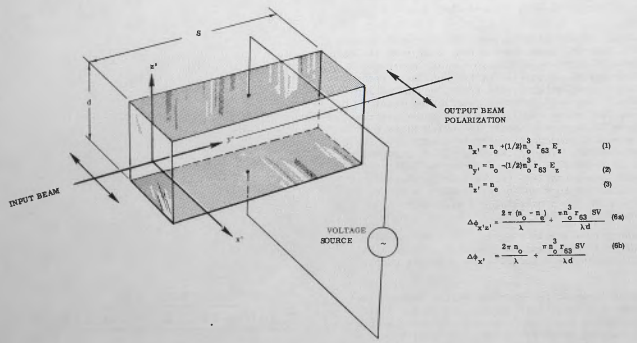

Figure 2 Transverse Field Electro-Optical Modulator

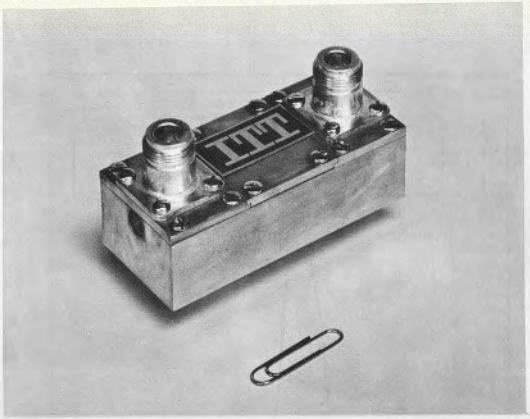

Figure 3 ITT Transverse Field Modulator Model EOM-3

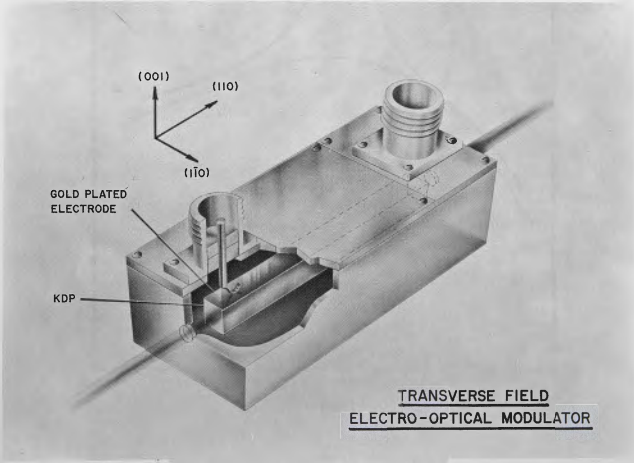

Figure 4 Transverse Field Electro-Optical Modulator

Figure 5 EOM-3 Performance Characteristics

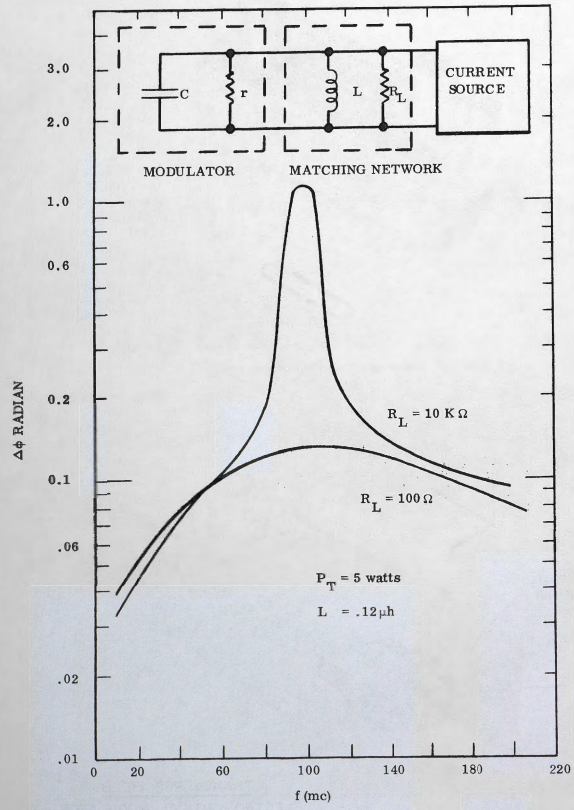

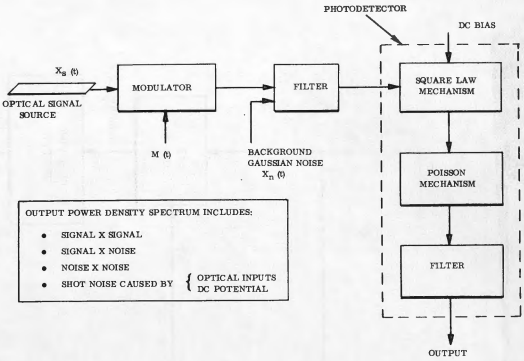

Figure 6 Model for S/N Derivation

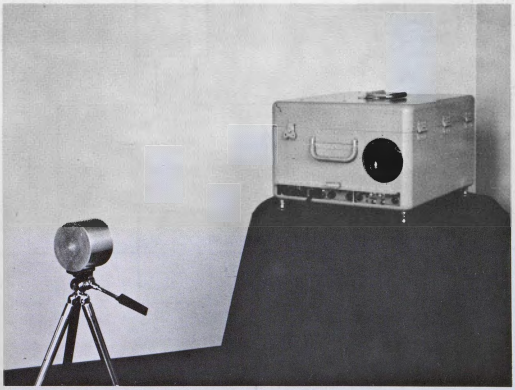

Figure 7 EODARS Breadboard

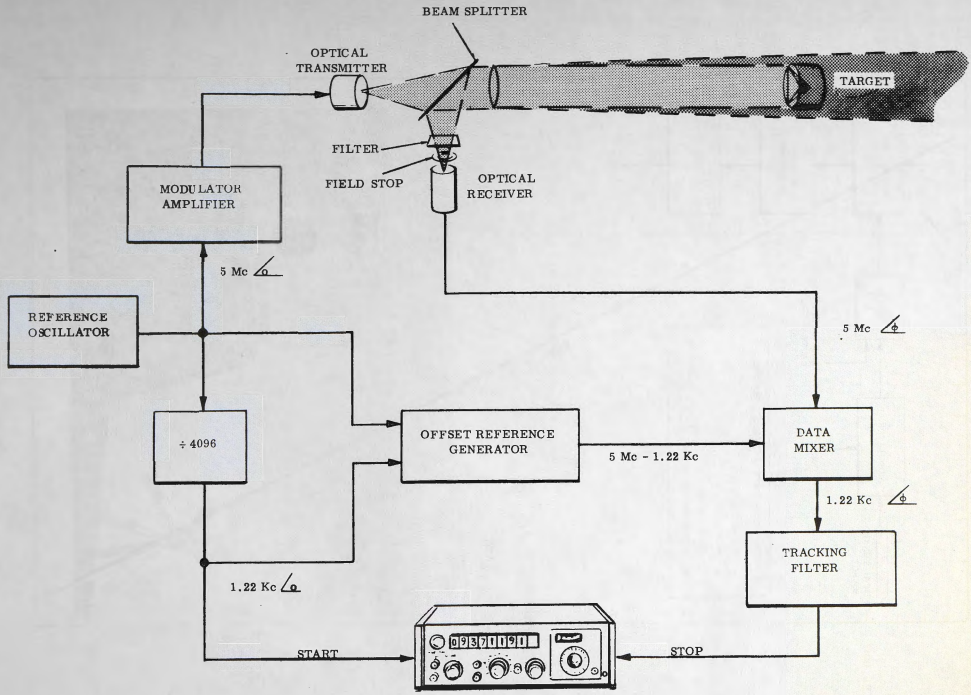

Figure 8 Simplified EODARS Block Diagram

Figure 9 Phase Jitter vs Signal-to-Noise Ratio

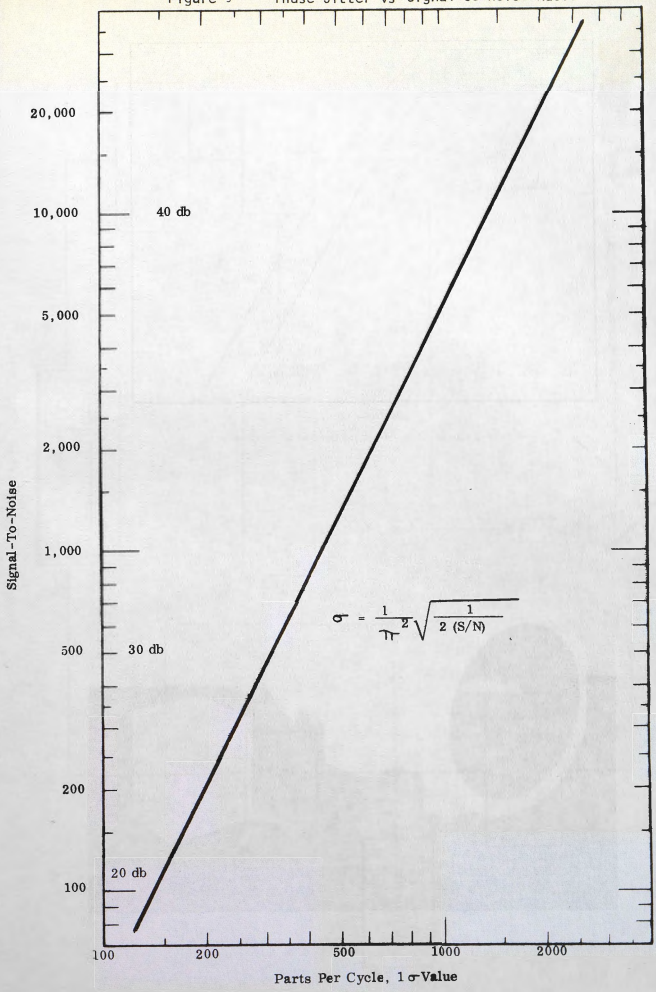

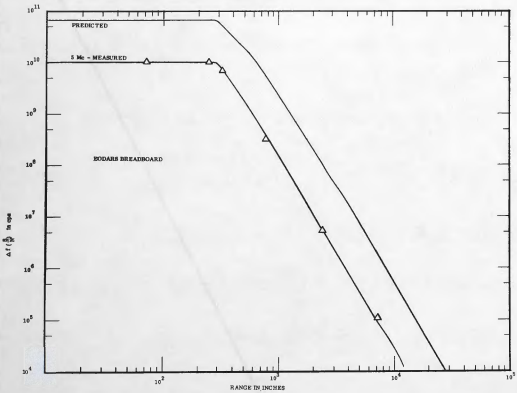

Figure 10 Comparison of Analytical and Experimental Performance

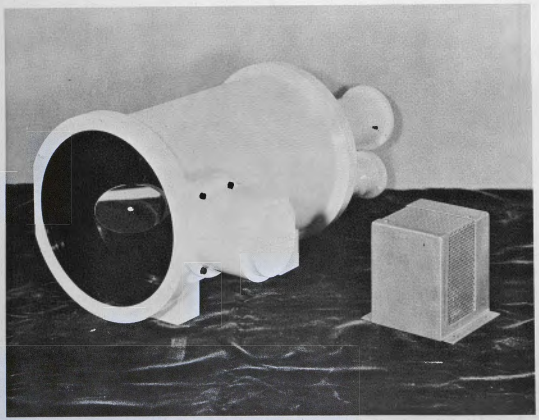

Figure 11 Prototype Optical Rendezvous Guidance System

RENDEZVOUS GUIDANCE SYSTEM

- MEASURES RANGE, RANGE RATE, X AND Y ANGLES, AND ANGLE RATE
- WILL RANGE AND TRACK TO 120 KILOMETERS
- RANGE ACCURACY — *1/2% FROM 120 km TO 3 km*; *10 cm FROM 3 km TO DOCKING*
- ANGLE ACCURACY — *10 ARC SECONDS*
- SIZE — *0.025 CUBIC METER (1 CUBIC FOOT)*
- WEIGHT — *35 POUNDS*
- POWER — *15 WATTS*

Figure 12 Rendezvous Guidance System

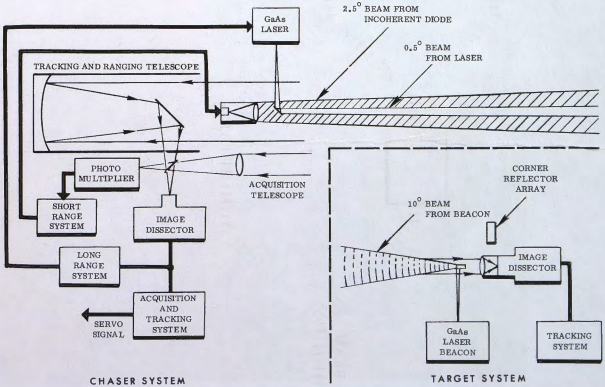

Figure 13 Rendezvous Guidance System Block Diagram

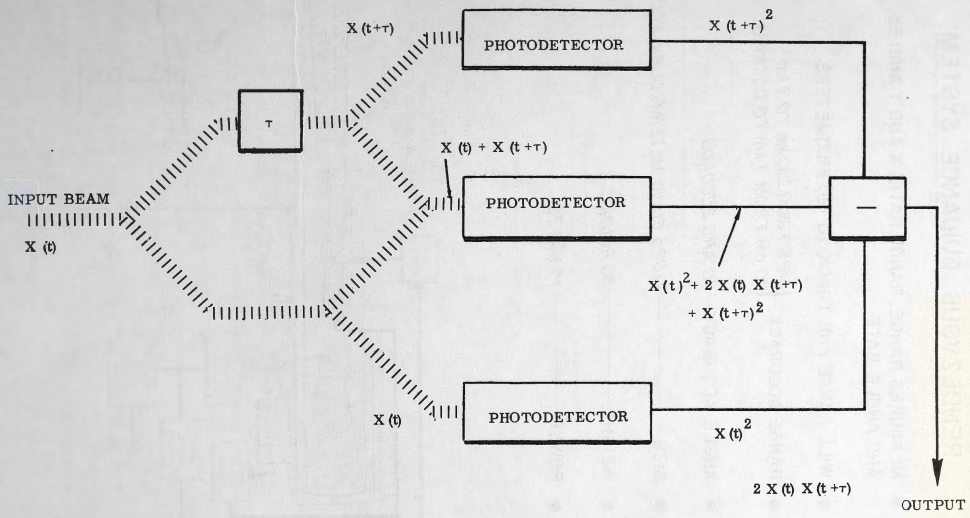

Figure 14 Optical Autocorrelator Schematic

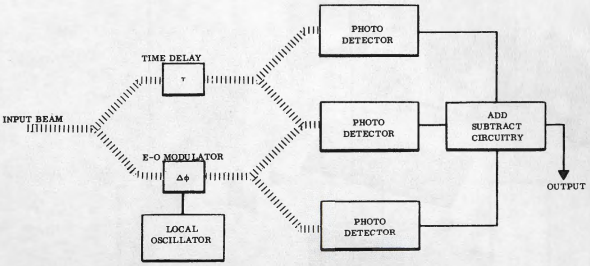

The frequency translated output signal is proportional to the first order Bessel Function Product:

$$J_1(k_r)^2 \, J_1\left(2k_t \sin\frac{\nu\tau}{2}\right)^2$$

where

k_r = modulation index of local modulator

k_t = modulation index of transmitter modulator

ν = transmitted subcarrier frequency

τ = interferometric time delay

Figure 15 Optical Autocorrelator with Local Modulator

Figure 16 Electro-Optical "Front End"

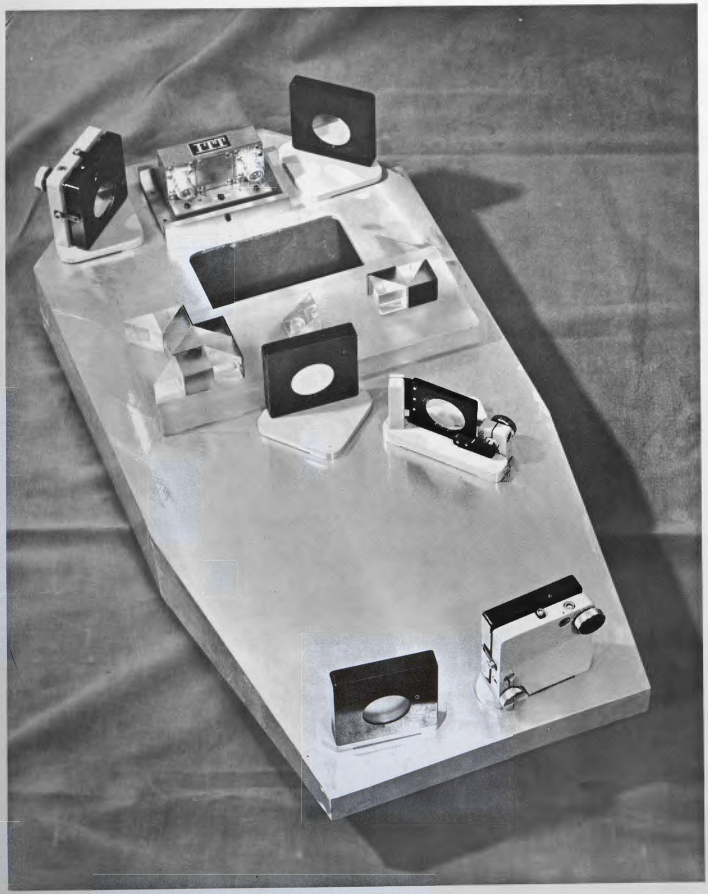

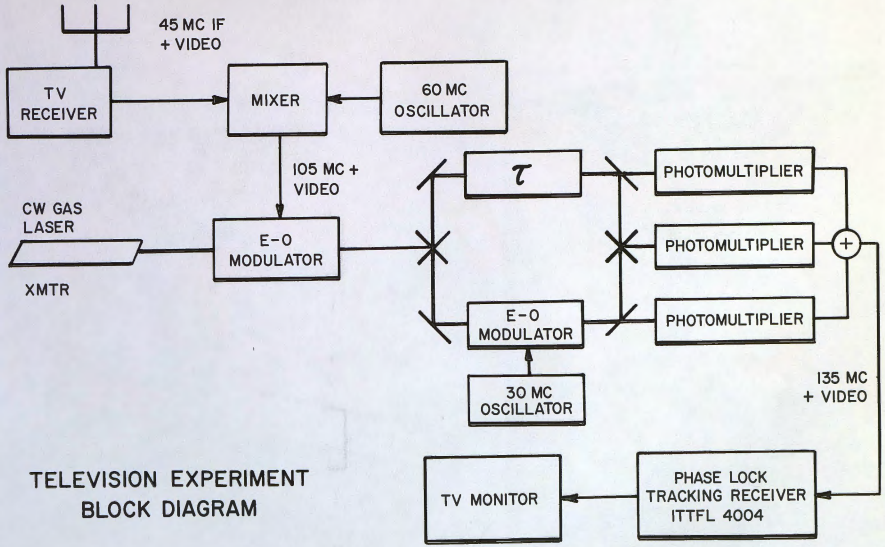

Figure 17 Television Experiment Block Diagram

Figure 18 Electro-Optical Transmitter

Figure 19 Electro-Optical Receiver